https://doi.org/10.1016/j.measurement.2019.107409

Development and Application of New FBG Mini Tension Link Transducers for Monitoring Dynamic Response of a Flexible Barrier under Impact Loads

by

Jie-Qiong QIN[1]

(Corresponding Author, PhD)

[1]Department of Civil and Environmental Engineering

The Hong Kong Polytechnic University, Hung Hom, Kowloon, Hong Kong, China

Email: jieqiong.qin@connect.polyu.hk

Jian-Hua YIN[1]

(PhD and Chair Professor of Soil Mechanics)

[1]Department of Civil and Environmental Engineering

The Hong Kong Polytechnic University, Hung Hom, Kowloon, Hong Kong, China

Tel: (852) 2766-6065, Fax: (852) 2334-6389, Email: cejhyin@polyu.edu.hk

Zhuo-Hui ZHU[1]

(PhD)

[1]Department of Civil and Environmental Engineering,

The Hong Kong Polytechnic University, Hung Hom, Kowloon, Hong Kong. China

Email: zhuo-hui.zhu@connect.polyu.hk

and

Dao-Yuan TAN[1]

(PhD)

[1]Department of Civil and Environmental Engineering,

The Hong Kong Polytechnic University, Hung Hom, Kowloon, Hong Kong. China

Email: t.daoyuan@connect.polyu.hk

Manuscript submitted to *Measurement* for possible publication as a *Technical Paper*

December 2019

Abstract

Flexible barriers, as an effective protective measure to mitigate landslide hazards, have attracted a lot of interest from the geotechnical community. The dynamic response of flexible barriers subjected to impact loads is of great concern. However, the forces developed on ring-net barriers during impacts have not been effectively measured and the dynamic behavior of barriers has not been fully understood. In this study, new mini tension link transducers based on fiber Bragg grating (FBG) sensing technology are uniquely developed to both link adjacent rings of a flexible barrier and measure the forces between rings. Besides, a novel monitoring system based on the new FBG mini tension link transducers is established for detecting dynamic response of a flexible barrier under impact loads. Calibration results of the FBG mini tension link transducers demonstrate that the wavelength shift of the FBG sensor has a linear relationship with the applied force with high accuracy. A single boulder impact test and a debris flow impact test were conducted to investigate the performance of the FBG-based system. The results reveal that the FBG mini tension link transducers are capable of capturing the evolution of the forces between rings of the flexible barrier, and the FBG-based system can be used for monitoring the dynamic response of the flexible barrier under impact loads.

Keywords: FBG; Tension link; Dynamic response; Flexible barrier; Boulder; Debris flow; Impact

1. Introduction

Landslides, such as rockfalls, rock avalanches, gravel flows, debris flows, and debris avalanches [1], are one of the most common geological hazards, which caused severe damages to structures and even a number of fatalities [2,3]. Over the last few decades, the awareness of the demand for mitigation of landslides has greatly increased, and a variety of landslide mitigation measures (e.g. concrete check dams, retaining walls, ground anchors, etc.) and monitoring systems have been investigated [4-10]. In recent years, flexible barriers have attracted a lot of interest from the geotechnical community and are widely regarded as an effective protective measure to mitigate landslide hazards by arresting the falling rocks and debris [11-13].

A flexible barrier system is typically composed of a ring-net barrier, supporting ropes, energy dissipating devices, steel posts, and retaining cables. By comparison with conventional concrete retaining structures, flexible barriers have the advantages of cost-effective design, ability of permeability, slight site disturbance, and easy construction on natural terrain. Moreover, the large deformation of flexible barriers prolongs the duration of impact process and reduces the maximum impact forces exerted on the barriers [14]. The performance of flexible barriers subjected to impact loads has been investigated by full-scale impact tests [15-17] and physical model impact tests [18-20]. However, in most studies, the impact behavior of flexible barriers was merely evaluated based on the measured forces developed in support ropes and/or retaining cables by load cells. In fact, in comparison to those supporting components, the ring-net barrier, which absorbs the majority of impact energy due to its large deformation, is the foremost component of a flexible barrier system. However, the forces developed on ring-net barriers during impacts have not been effectively measured and the dynamic behavior of barriers has not been fully understood in the literature. Hence, an effective approach to force measurement of ring-net barriers is required, thereby helping deeply understand the impact behavior of flexible barriers.

In the past decade, fiber Bragg grating (FBG), as a popular fiber optic sensing (FOS) technology, has been effectively employed in in-situ monitoring [9,21-25] and early warning of landslides [26,27] owing to its superiority in small size, high accuracy and resolution, good reliability, immunity to electromagnetic interference (EMI), and capacity of multiplexing [28-32]. Besides, the application of FBG sensing technology has also been extended to monitoring the dynamic behavior of supporting components of a flexible barrier system. Huang *et al*. [33] designed FBG tension sensors to record the dynamic forces on anchor ropes during the full-scale impact test of rockfall protection barriers for investigating the impact behavior of the barriers. Guo *et al*. [34] presented a sensing detection system based on FBG sensing technology for rockfall protective barriers. By making use of this sensing detection system, the dynamic force response of steel strands and the strain response of supporting I-beams were captured to study and evaluate the performance of the protective barrier upon rockfall impact.

In this study, we explore the potential applications of FBG sensing technology in dynamic monitoring of a flexible barrier against landslide hazards. As mentioned, there is a demand for an effective approach to force measurement of ring-net barriers. In this connection, new FBG mini tension link transducers are uniquely designed and developed to both link adjacent rings of a flexible barrier and measure the forces between rings by means of a sensing bar with U-sharped openings at two ends. Moreover, to further detect the dynamic response of an entire flexible barrier under impact loads, a novel monitoring system based on the developed FBG mini tension link transducers is established. The performance of the FBG-based monitoring system during dynamic impacts has been investigated through the single boulder impact test and the debris flow impact test. This novel monitoring approach helps to capture the evolution of the forces between rings of the flexible barrier and the force distribution on the flexible barrier under impact loads, to evaluate the performance of a flexible barrier during the impact of a rockfall or a debris flow, and to deeply understand the interaction mechanism between the impact material and barrier.

2. Development of the new FBG mini tension link transducers

2.1. Principle of FBG sensing technology

The first FBG sensor was fabricated by Hill *et al.* [35] based on their discovery of the photosensitivity phenomenon in Ge-doped core optical fibers. The Bragg grating can be photo-inscribed into a segment of Ge-doped single-mode silica fiber by exposing the fiber core to a spatial pattern of intense ultraviolet (UV) light, and a periodic modulation of the core refractive index is accordingly formed in the fiber [36,37]. In accordance with Bragg's law, when light from a spectrally broadband source is injected into the FBG sensor, a narrow spectral component at the Bragg wavelength is reflected by the grating, as shown in Fig. 1. The reflected

Bragg wavelength (λ_B) is determined by both the effective core refractive index of the fiber (n_e) and the grating period (Λ), and the relationship is expressed as follows [38]:

$$\lambda_B = 2n_e\Lambda \tag{1}$$

The Bragg wavelength is affected by strain and temperature. A change in strain causes both the change in the grating period due to physical elongation of the fiber and the change in fiber refractive index due to photo-elastic effect, and a variation in temperature produces both the thermal expansion of the fiber and the change in fiber refractive index due to thermo-optic effect [38]. For a single mode silica fiber, the Bragg wavelength shift ($\Delta\lambda_B$) induced by the strain change ($\Delta\varepsilon$) and temperature variation (ΔT) is given by [38,39]:

$$\frac{\Delta\lambda_B}{\lambda_{B0}} = \left(1 - p_e\right)\Delta\varepsilon + \left(\alpha + \xi\right)\Delta T = c_\varepsilon\Delta\varepsilon + c_T\Delta T \tag{2}$$

where λ_{B0} is the Bragg wavelength at initial state; p_e is the effective photo-elastic coefficient; α is the thermal expansion coefficient of the fiber material; ξ is the thermo-optic coefficient; c_ε and c_T represent the coefficients of strain and temperature with the typical values of 0.78 and $6.67\times10^{-6}/{}^\circ C$, respectively. It is noted that temperature compensation can be achieved by placing an additional FBG sensor, free of any mechanical strain, to the same temperature field. With the temperature variation (ΔT) obtained by the additional FBG sensor, the strain change ($\Delta\varepsilon$) can be calculated using the following equation:

$$\Delta\varepsilon = \frac{1}{c_\varepsilon}\left(\frac{\Delta\lambda_B}{\lambda_{B0}} - c_T\Delta T\right) \tag{3}$$

2.2. Design of the FBG mini tension link transducers

The specially designed FBG mini tension link transducers are utilized as connectors to both link adjacent rings of a flexible barrier and measure the forces between rings within a certain area of a flexible barrier, and thus the dynamic response of ring-net barriers during impact can be easily recorded and analyzed. Fig. 2(a) depicts the schematic diagram of the designed FBG mini tension link transducers. The sensing element is a sensing bar (40 mm long, 20 mm wide, and 10 mm thick) with two U-shaped openings at both ends for rings connection. An FBG sensor was bonded on the surface of the sensing bar by epoxy adhesive. In view of multiplexing, the FBG sensor has two FC/APC connectors at both ends that can be employed for a series connection. Finally, the sensing bar was encapsulated by a metal tube for protection, as shown in Fig. 2(b).

According to Hooke's law, when a tensile force (F_t) is exerted on an FBG mini tension link transducer, the axial strain (ε) generated on the surface of the sensing bar is determined by:

$$\varepsilon = \frac{F_{\mathrm{t}}}{EA} \tag{4}$$

where E is the elastic modulus of the sensing bar material and A is the cross-sectional area of the sensing bar. Combining Eqs. (3) and (4), the relationship between the applied tensile force and Bragg wavelength shift is expressed as:

$$\Delta F_t = EA \times \Delta\varepsilon = \frac{EA}{c_\varepsilon}\left(\frac{\Delta\lambda_B}{\lambda_{B0}} - c_T \Delta T\right) \tag{5}$$

In this study, the sensing elements of the FBG mini tension link transducers were made of 316 stainless steel (elastic modulus $E = 196\ GPa$ and yield strain $\varepsilon_y = 1050\ \mu\varepsilon$). According to Eq. (4), the allowable bearing capacity of the designed FBG mini tension link transducer is calculated to be 20 kN based on the mechanical properties of 316 stainless steel and dimensions of the sensing bar (as shown in Fig. 2(a)).

2.3. Calibration of the FBG mini tension link transducers

2.3.1. Test setup and procedure

Tensile tests for calibration of the FBG mini tension link transducers were conducted successively on the universal testing machine (UTM) in Concrete Technology Laboratory of The Hong Kong Polytechnic University, as presented in Fig. 3(a). The UTM controlled the applied forces which changed from 0 to 20 kN at 4 kN increments, and a load cell with a capacity of 50 kN was used to record the applied forces. Each FBG mini tension link transducer was tested with two loading-unloading cycles to examine the repeatability. The load cell was connected to a data acquisition device (model NI PXIe-4331, National Instruments), and the FBG mini tension link transducers were interrogated by an optical sensing interrogator (model si255, Micron Optics). It is noted that the calibration tests were performed at a constant temperature of $20\,°C$. Therefore, the temperature-induced wavelength shift can be neglected, and thus Eq. (5) can be simplified as:

$$\Delta F_t = \frac{EA}{c_\varepsilon \lambda_{B0}} \Delta\lambda_B \tag{6}$$

2.3.2. Test results and discussion

The calibration results of three FBG mini tension link transducers (FBG-TL 1/2/3) with the corresponding initial wavelength of 1525.658 nm, 1540.653 nm, and 1555.651 nm are discussed here. Fig. 3(b) plots the calibration results of the FBG mini tension link transducers (FBG-TL 1/2/3) respectively. The figure demonstrates a good repeatability of the designed FBG mini tension link transducers and a linearity of the shift in Bragg wavelength and applied force which agrees well with the theoretical analysis exhibited by Eq. (6). Linear transfer functions with good coefficient of determination (COD) values (greater than 0.999) are provided by adopting the least-squares method. The sensitivity ($\Delta\lambda_B/\Delta F_t$) of each FBG mini tension link transducer can be obtained from the linear transfer function. The coefficient for converting the wavelength shift into force can be accordingly determined by the reciprocal of sensitivity, and the corresponding theoretical value can be calculated based on Eq. (6). The coefficients determined by calibration results and theoretical calculations are compared and summarized in Table 1. It is found that for each FBG mini tension link transducer, the coefficient obtained from calibration results is in good accordance with the theoretical value with a relative error of less than 5%. For calibration results of the other FBG mini tension link transducers, the relative error is also within 5%. When the FBG sensors are interrogated by the optical sensing interrogator (model si255, Micron Optics) which has a wavelength resolution of 1 pm (i.e. 0.001 nm), the force resolution of the designed FBG mini tension link transducers is 0.03 kN.

3. Application of the new FBG mini tension link transducers in impact tests

In this study, a large-scale physical model was designed for the impact tests and constructed in Road Research Laboratory of The Hong Kong Polytechnic University. A single boulder impact test and a debris flow impact test were performed in this large-scale physical model. The novelty of the impact tests lies in the adoption of the newly developed FBG mini tension link transducers on ring-net barrier. This is the first attempt to measure the forces between rings and monitor the dynamic response of the entire barrier during the impact tests. This work sets the foundation for studying the impact behavior of a flexible barrier against landslide hazards.

3.1. Large-scale physical model

The large-scale physical model contains three main components: a storage container, a chute, and a flexible barrier system, as shown in Fig. 4(a). The storage container with a volume capacity of 5 m^3 was mounted above the chute at the height of 3.6 m. This container is of an inclined base that can contribute to motivating the movement of test materials and a flip-up trapdoor with an elaborately designed operation system that can achieve a quick release of the test materials. The chute has a width of 1.5 m, a length of 6.8 m, and an inclination angle of 35°. Tempered glass is used as transparent sidewalls to form a channelized chute and provide a clear viewing perspective on the motion of test materials. The flexible barrier system is located at the bottom of the chute. As shown in Fig. 4(b), it consists of a prototype flexible ring-net barrier (ring-net type ROCCO®7/3/300, GEOBRUGG Ltd.), support ropes, a pair of steel posts, and retaining cables. The steel posts, perpendicular to the chute, are hinged to the foundation and connected with the retaining cables at their upper ends. The support ropes are suspended by the steel posts to form a frame for a ring-net barrier. In the debris flow impact test, a second layer of a chain-link mesh with smaller mesh size was utilized to prevent high discharge of finer materials.

3.2. Instrumentation

Two different barrier configurations were employed in the single boulder impact test and the debris flow impact test respectively, as illustrated in Fig. 5. In the single boulder impact test, a 2.48 m wide and 1.48 m high barrier was adopted and equipped with ten FBG mini tension link transducers. In the debris flow impact test, a 2.48 m wide and 0.915 m high barrier was utilized to ensure the overflow of debris flow and equipped with twelve FBG mini tension link transducers. Besides, an additional FBG mini tension link transducer was placed close to the barrier and isolated from any mechanical strain for temperature compensation. The FBG mini tension link transducers were interrogated by an optical sensing interrogator (model si255, Micron Optics) capable of recording at 1 kHz and measuring simultaneously on 16 parallel channels. The si255 was connected to a computer utilizing ENLIGHT (sensing analysis software, Micron Optics) for display and data storage. In both impact tests, the frequency of data acquisition was set at 1 kHz. Two high-speed cameras (model MacroVis EoSens, HSVISION GmbH) with a resolution of 1696 × 1710 pixels at 523 frames per second (fps) were settled in front and side of the flexible barrier system respectively and directed at the location of barrier to capture the interaction between the impact mass and flexible barrier during the impact process.

3.3. Test materials and procedures

A spherical boulder with a diameter of 600 mm and a density of 2650 kg/m^3 was used in the single boulder impact test. In the debris flow impact test, the debris flow material comprised Completely Decomposed Granite (CDG), gravel, and water, which were stirred up into a saturated and homogeneous mixture with a total volume of 2.62 m^3 and water content of 24.5% (percentage of mass). The gravels range in size from 20 to 30 mm. In both tests, the materials were quickly released from the storage container by flipping up the trapdoor within 0.5 s, and then the materials moved along the chute until impacting the barrier. Figure 6 shows the experimental process. The data from the FBG mini tension link transducers was recorded before the release of materials to acquire the initial values and the high-speed cameras were triggered at the moment of materials releasing to capture the motion of materials and the impact process.

4. Test results and discussions

Typical video recordings (front and side views) from the high-speed cameras are shown in Fig. 7 for the two tests. Different impact characteristics of the single boulder and debris flow were identified from the impact tests. The single boulder produced a transient impact with a concentrated load and resulted in a large deformation of the barrier due to its high kinetic energy. By contrast, debris flow created continuous impacts accompanied with the deposition of the debris, and the impact loads generated by debris flow were complicated owing to the rheology of the mixture. Based on the test data collected by the FBG mini tension link transducers in the single boulder impact test and the debris flow impact test, the dynamic response of the flexible barrier, including the forces developed between rings and the force distribution in the measurement area of the barrier, was analyzed for both tests.

4.1. Forces between the rings of barriers

Time histories of the measured forces between rings of the flexible barrier for the single boulder impact test and the debris flow impact test are presented in Figs. 8 and 9, respectively. In Fig. 8, the initial time ($t = 0\ s$) indicates the moment of the first contact between the spherical boulder and ring-net barrier. It is observed that forces were first detected in the bottom FBG mini tension link transducers (FBG-TL 5/6), and then captured by the upper FBG mini tension link transducers successively. With the forward movement of the spherical boulder, the deformation of the barrier and the forces between rings increased dramatically within 0.14 s. The maximum force measured by each FBG mini tension link transducer is provided in the figure. It is found that at the same height, the maximum force measured by the FBG mini tension link transducer in the right half of barrier (FBG-TL 1/2/3/4/5) is larger, which results from that the impact location of the spherical boulder was not exactly in the center of the barrier. After reaching the maximum deformation of the barrier, the spherical boulder was bounced off, and thus the measured forces approximately decreased to 0 kN. The spherical boulder impacted the barrier again with a lower level of kinetic energy at 0.93 s and was eventually trapped by the barrier.

In Fig. 9, the initial time ($t = 0\ s$) means the moment when the first flow front reached the location of barrier. In the first 3.5 s, the great majority of debris flow passed from the basal opening between the chute base and the barrier due to the insufficient flow height. Hence, the measured forces between the rings were very small and slightly fluctuant in this period. With the growth of flow height, the debris flow impacted the barrier and the debris gradually deposited behind the barrier. The forces were detected in the FBG mini tension link transducers successively (from the bottom up), which is similar to the observation in the single boulder impact test. Upon impact, the measured forces rapidly rose to peak values that are shown in the figure. It is found that the maximum forces in the central area of barrier (FBG-TL 1-8) are larger than those in the side area (FBG-TL 9-12). After the peak values, all the forces exhibited a sudden drop that may be attributed to the deformation recovery of the rotatable steel posts, and then experienced a rapid increase until a static state was reached.

It is found that the time histories of the forces between rings obtained by the designed FBG mini tension link transducers in this single boulder impact test show the same trend with the force time histories of anchorages acquired by conventional load cells [16] and the force time histories of steel strands provided by FBG force transducers [34], and the evolution of the forces between rings acquired by the designed FBG mini tension link transducers in this debris flow impact test have a consistent trend with those of support rope forces obtained by conventional load cells in the full-scale impact tests [14,15] and the centrifuge model impact tests [20]. It proves that the FBG mini tension link transducers can be utilized for effectively measuring the dynamic forces between rings of the ring-net barrier. Moreover, measurement of forces between rings can provide valuable information on loading assessment of the barrier, such as the location of maximum force, which greatly helps in design and maintenance of the barrier.

4.2. Force distribution in the barriers

Figures 10 and 11 depict the force distribution in the measurement area of the barrier at typical time points (indicated in Figs. 8 and 9) for the single boulder impact test and the debris flow impact test, respectively. The axes of horizontal position and height refer to the x and y axes as illustrated in Fig. 5. It can be seen that during the single boulder impact, the largest force successively occurred in the bottom (0.048 s), middle (0.099 s) and top (0.139 s) of the monitoring area of the barrier. With the forward and upward movement of the spherical boulder, the upper part of the barrier experienced lager force. After the impact (0.188 s), the top monitoring area of the barrier still sustained larger force than the rest until the spherical boulder was entirely detached from the barrier. Since the impact load of the spherical boulder can be typically simplified as a concentrated force, the force distribution of the barrier is relatively vertically symmetrical.

As for the force distribution of the barrier upon debris flow impact, it is observed that the bottom of the barrier experienced larger force at 3.735 s due to the impact of small debris surges and the debris deposition. With the growth of flow height, a large debris surge was generated and impacted on the center-right area of the barrier (observed in video recordings), which resulted in the dramatic increase of forces in this area (3.815 s). However, the impact of the larger debris surge had less influence on the bottom and side of the barrier. It is revealed that the impact area loads from debris flow are complicated and non-uniform, and the impact area and location have significant effects on the dynamic force response of flexible barriers. During the period of posts deformation recovery (3.980 s), the forces on the barrier were deceased to smaller values. After a static state was reached (5.300 s), the forces on the barrier were constant and induced by the deposited debris only.

By making use of the newly developed FBG mini tension link transducers, the force distribution on flexible barrier under impact loads was obtained for the first time. It is favorable for evaluating the performance of a ring-net barrier during dynamic impacts, estimating the impact force imposed on a flexible barrier, and understanding the impact mechanism of boulders or complicated geophysical flows on a flexible barrier.

5. Summary and conclusions

In this study, the design, calibration and application of the FBG mini tension link transducers for measuring the forces between rings of the flexible barrier have been presented. The working principle of FBG sensing technology is introduced. The calibration tests of the FBG mini tension link transducers were performed on the universal testing machine in laboratory. Moreover, the FBG mini tension link transducers were applied to the large-scale physical model impact tests for investigating the dynamic response of the flexible barrier under impact loads. A single boulder impact test and a debris flow impact test were carried out. The summary and conclusions are listed as follows:

(a) Calibration results demonstrate that the relationship between the wavelength shift of the FBG mini tension link transducers and the applied force exhibits good linearity with high accuracy. The calibration coefficients are in good accordance with the theoretical values with a relative error of less than 5%.

(b) The force resolution of 0.03 kN can be obtained when the FBG mini tension link transducers are interrogated by an optical sensing interrogator with a 1 pm wavelength resolution.

(c) By comparison with previous studies, it is verified that the FBG mini tension link transducers have a good performance and reliability to capture the evolution of the forces between rings of the flexible barrier. The measurement of forces between rings can provide valuable information for loading assessment of the barrier, such as the location of maximum force, which greatly helps in design and maintenance of the barrier.

(d) Based on the force measurements by the FBG mini tension link transducers, the force distribution with height and horizontal position of the flexible barrier can be obtained, which is conducive to deeply understanding the interaction mechanism between impact materials and barriers.

Hence, the work presented in this study is significant and meaningful. It is worth applying the newly developed FBG mini tension link transducers to field monitoring and model tests in the future.

Acknowledgements

The work in this paper is supported by a CRF project (Grant No.: PolyU 12/CRF/13E) from

Research Grants Council (RGC) of Hong Kong Special Administrative Region Government (HKSARG) of China. The authors also acknowledge the financial supports from Research Institute for Sustainable Urban Development of The Hong Kong Polytechnic University (PolyU), Research Centre for Urban Hazards Mitigation of Faculty of Construction and Environment of PolyU, and PolyU grants (1-ZVCR, 1-ZVEH, 4-BCAU, 4-BCAW, 5-ZDAF, G-YN97).

References

[1] O. Hungr, S.G. Evans, M.J. Bovis, J.N. Hutchinson, A review of the classification of landslides of the flow type. Environmental & Engineering Geoscience, 7 (2001) 221-238.

[2] D.N. Petley, S.A. Dunning, N.J. Rosser, O. Hungr, The analysis of global landslide risk through the creation of a database of worldwide landslide fatalities. Landslide risk management. Balkema, Amsterdam, (2005) 367-374.

[3] O. Kjekstad, L. Highland, Economic and social impacts of landslides. Landslides–Disaster Risk Reduction. Berlin, Heidelberg, (2009) 573-587.

[4] M.E. Popescu, K. Sasahara, Engineering measures for landslide disaster mitigation. Landslides–Disaster Risk Reduction. Berlin, Heidelberg, (2009) 609-631.

[5] K.Y. Choi, R.W. Cheung, Landslide disaster prevention and mitigation through works in Hong Kong. Journal of Rock Mechanics and Geotechnical Engineering, 5 (2013) 354-365.

[6] P. Giri, K. Ng, W. Phillips, Wireless sensor network system for landslide monitoring and warning. IEEE Transactions on Instrumentation and Measurement, 99 (2018) 1-11.

[7] V. Van Khoa, S. Takayama, Wireless sensor network in landslide monitoring system with remote data management. Measurement, 118 (2018) 214-229.

[8] Z. Yu, H. Dai, Q. Zhang, M. Zhang, L. Liu, J. Zhang, X. Jin, High-resolution distributed strain sensing system for landslide monitoring. Optik, 158 (2018) 91-96.

[9] H.F. Pei, S.Q. Zhang, L. Borana, Y. Zhao, J.H. Yin, Slope stability analysis based on real-time displacement measurements. Measurement, 131 (2019) 686-693.

[10] C. Liu, Z. Jiang, X. Han, W. Zhou, Slope displacement prediction using sequential intelligent computing algorithms. Measurement, 134 (2019) 634-648.

[11] A. Roth, C. Wendeler, F. Amend, Use of properly designed flexible barriers to mitigate debris flow natural hazards. GeoFlorida 2010: Advances in Analysis, Modeling & Design, (2010) 3207-3216.

[12] A. Bichler, D. Yonin, G. Stelzer, Flexible debris flow mitigation: introducing the 5.5 mile debris fence. Landslides and engineered slopes: protecting society through improved understanding. New York, (2012) 1955-1960.

[13] J.S. Kwan, S.L. Chan, J.C. Cheuk, R.C.H. Koo, A case study on an open hillside landslide impacting on a flexible rockfall barrier at Jordan Valley, Hong Kong. Landslides, 11 (2014) 1037-1050.

[14] C. Wendeler, A. Volkwein, A. Roth, M. Denk, S. Wartmann, Field measurements and numerical modelling of flexible debris flow barriers. Debris-Flow Hazards Mitigation: Mechanics, Prediction, and Assessment. Millpress, Rotterdam, (2007) 681-687.

[15] L. Bugnion, C. Wendeler, Shallow landslide full-scale experiments in combination with testing of a flexible barrier. WIT Transactions on Engineering Sciences, 67 (2010) 161-173.

[16] G. Gottardi, L. Govoni, Full-scale modelling of falling rock protection barriers. Rock

mechanics and rock engineering, 43 (2010) 261-274.

[17] Z.X. Yu, Y.K. Qiao, L. Zhao, H. Xu, S.C. Zhao, Y.P. Liu, A simple analytical method for evaluation of flexible rockfall barrier part 2: application and full-scale test. Advanced Steel Construction, 14 (2018) 142-165.

[18] W. Ashwood, O. Hungr, Estimating total resisting force in flexible barrier impacted by a granular avalanche using physical and numerical modeling. Canadian Geotechnical Journal, 53 (2016) 1700-1717.

[19] K.S. Lee, S.H. Cho, J.H. Kim, B.S. Yoo, Impact force assessment of flexible debris-flow barriers using small-scale model test. International Journal of Mechanical and Production Engineering, 5 (2017) 46-50.

[20] D. Song, C.E. Choi, C.W.W. Ng, G.G.D. Zhou, Geophysical flows impacting a flexible barrier: effects of solid-fluid interaction. Landslides, 15 (2018) 99-110.

[21] A.B. Huang, J.T. Lee, Y.T. Ho, Y.F. Chiu, S.Y. Cheng, Stability monitoring of rainfall-induced deep landslides through pore pressure profile measurements. Soils and Foundations, 52 (2012) 737-747.

[22] A. Minardo, E. Catalano, A. Coscetta, G. Zeni, L. Zhang, C. Di Maio, R. Vassallo, R. Coviello, G. Macchia, L. Picarelli, L. Zeni, Distributed fiber optic sensors for the monitoring of a tunnel crossing a landslide. Remote Sensing, 10 (2018) 1291.

[23] Y. Zheng, D. Huang, L. Shi, A new deflection solution and application of a fiber Bragg grating-based inclinometer for monitoring internal displacements in slopes. Measurement Science and Technology, 29 (2018).

[24] H. Wu, Y. Guo, L. Xiong, W. Liu, G. Li, X. Zhou, Optical fiber-based sensing, measuring,

and implementation methods for slope deformation monitoring: a review. IEEE Sensors Journal, 19 (2019) 2786-2800.

[25] H. Xu, X. Zheng, W. Zhao, X. Sun, F. Li, Y. Du, B. Liu, Y. Gao, High precision, small size and flexible FBG strain sensor for slope model monitoring. Sensors, 19 (2019) 2716.

[26] M. Bellas, G. Voulgaridis, Study of the major landslide at the community of Ropoto, Central Greece, mitigation and FBG early warning system design. Innovative Infrastructure Solutions, 3 (2018) 30.

[27] Y. Hu, C. Hong, Y. Zhang, G. Li, A monitoring and warning system for expressway slopes using FBG sensing technology. International Journal of Distributed Sensor Networks, 14 (2018).

[28] H.H. Zhu, B. Shi, C.C. Zhang, FBG-based monitoring of geohazards: current status and trends. Sensors, 17 (2017) 452.

[29] S. Das, P. Saha, A review of some advanced sensors used for health diagnosis of civil engineering structures. Measurement, 129 (2018) 68-90.

[30] C. Hong, Y. Zhang, Y. Yang, Y. Yuan, A FBG based displacement transducer for small soil deformation measurement. Sensors and Actuators A: Physical, 286 (2019) 35-42.

[31] Y. Zheng, Z.W. Zhu, X. Yi, W.J. Li, Review and comparative study of strain–displacement conversion methods used in fiber Bragg grating-based inclinometers. Measurement, 137 (2019) 28-38.

[32] R. You, L. Ren, G. Song, A novel fiber Bragg grating (FBG) soil strain sensor. Measurement, 139 (2019) 85-91.

[33] J. Huang, Z. Zhou, D.S. Zhang, J.T. Chen, L.T. Li, X.W. Deng, Design and application of

a fiber bragg grating tension sensor for anchor rope. Advances in Mechanical Engineering, 2013 (2013) 995-1001.

[34] Y.X. Guo, D.S. Zhang, Z.D. Zhou, F.D. Zhu, L. Xiong, Development and commissioning of FBG sensors for impact test of rock fall protective barrier. Sensor Review, 34 (2014) 343-348.

[35] K.O. Hill, Y. Fujii, D.C. Johnson, B.S. Kawasaki, Photosensitivity in optical fiber waveguides: Application to reflection filter fabrication. Applied Physics Letters, 32 (1978) 647-649.

[36] G. Meltz, W. Morey, W.H. Glenn, Formation of Bragg gratings in optical fibers by a transverse holographic method. Optics Letters, 14 (1989) 823-825.

[37] K.O. Hill, B. Malo, F. Bilodeau, D.C. Johnson, J. Albert, Bragg gratings fabricated in monomode photosensitive optical fiber by UV exposure through a phase mask. Applied Physics Letters, 62 (1993) 1035-1037.

[38] W.W. Morey, G. Meltz, W.H. Glenn, Fiber optic Bragg grating sensors. Fiber Optic and Laser Sensors VII, 1169 (1989) 98-108.

[39] K.O. Hill, G. Meltz, Fiber Bragg grating technology fundamentals and overview. Journal of Lightwave Technology, 15 (1997) 1263-1276.

List of figure Captions

Fig. 1. Principle of FBG sensing technology

Fig. 2. Design of an FBG mini tension link transducer: (a) schematic diagram (all dimensions in mm) and (b) photograph

Fig. 3. Calibration of the FBG mini tension link transducers: (a) test setup and (b) test results

Fig. 4. Panorama of (a) the large-scale physical model for testing a flexible barrier under impact of a single boulder or debris flow and (b) the flexible barrier system

Fig. 5. Arrangement of FBG mini tension link transducers in a flexible barrier: (a) the single boulder impact test and (b) the debris flow impact test

Fig. 6. Experimental process: (a) before test, (b) door flipping up, and (c) material releasing

Fig. 7. Typical video recordings for: (a) the single boulder impact test and (b) the debris flow impact test

Fig. 8. Time histories of the measured forces (F_t) between rings of the flexible barrier for the single boulder impact test

Fig. 9. Time histories of the measured forces (F_t) between rings of the flexible barrier for the debris flow impact test

Fig. 10. Distribution of the forces between rings of the flexible barrier for the single boulder impact test

Fig. 11. Distribution of the forces between rings of the flexible barrier for the debris flow impact test

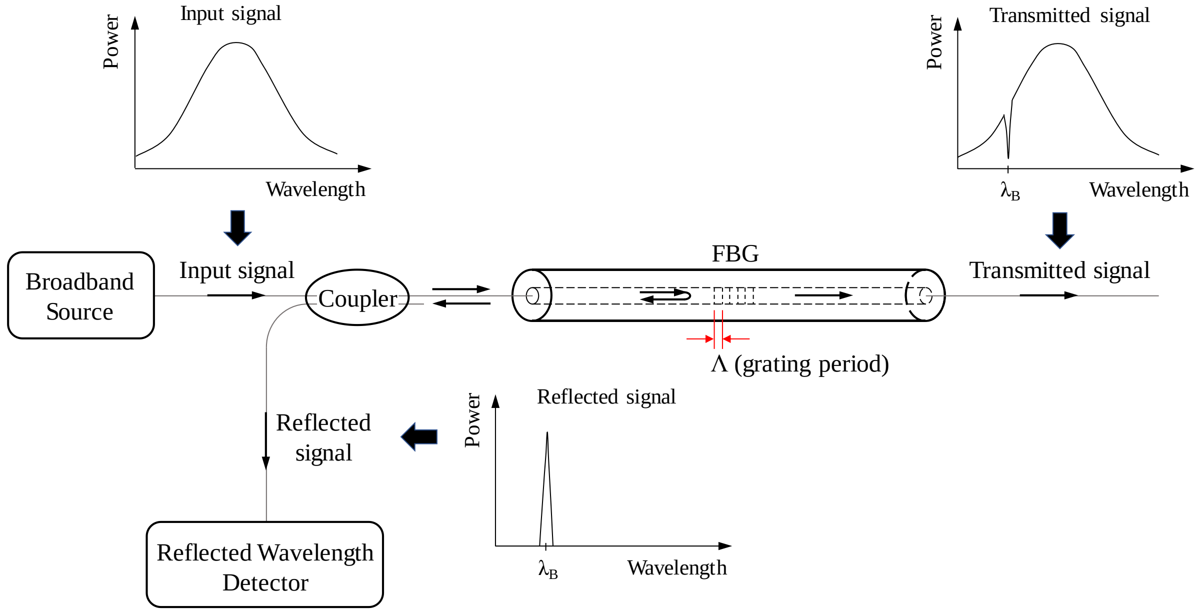

Fig. 1. Principle of FBG sensing technology

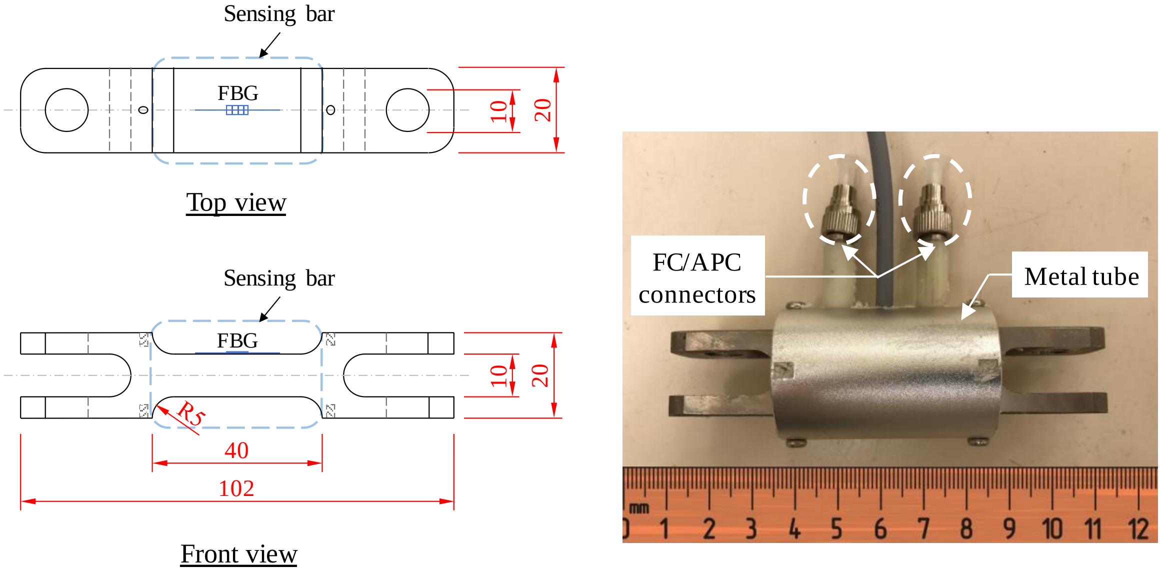

(a) (b)

Fig. 2. Design of an FBG mini tension link transducer: (a) schematic diagram (all dimensions in mm) and (b) photograph

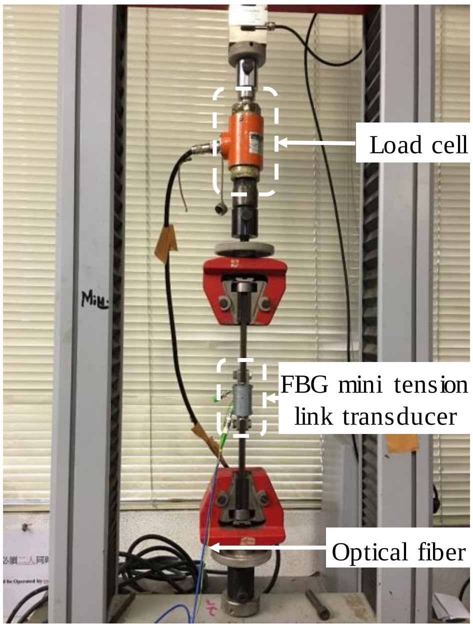

(a)

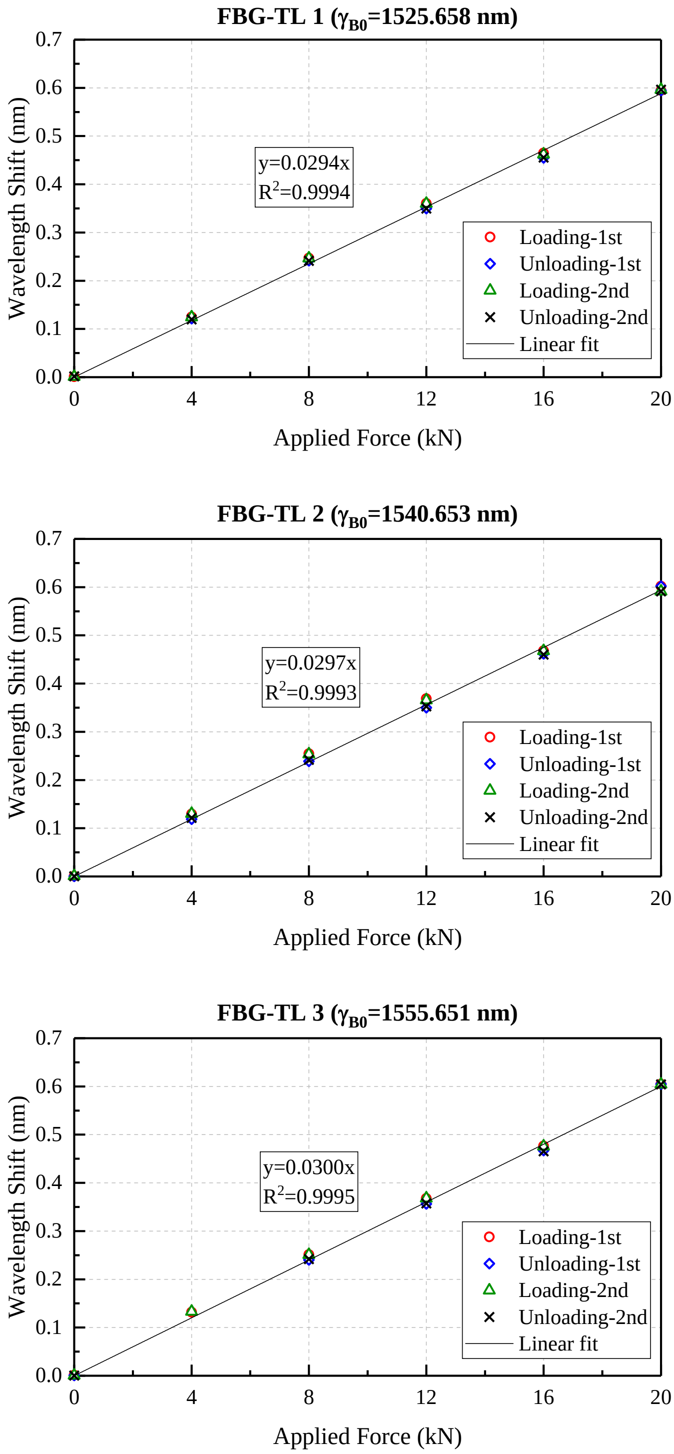

(b)

Fig. 3. Calibration of the FBG mini tension link transducers: (a) test setup and (b) test results

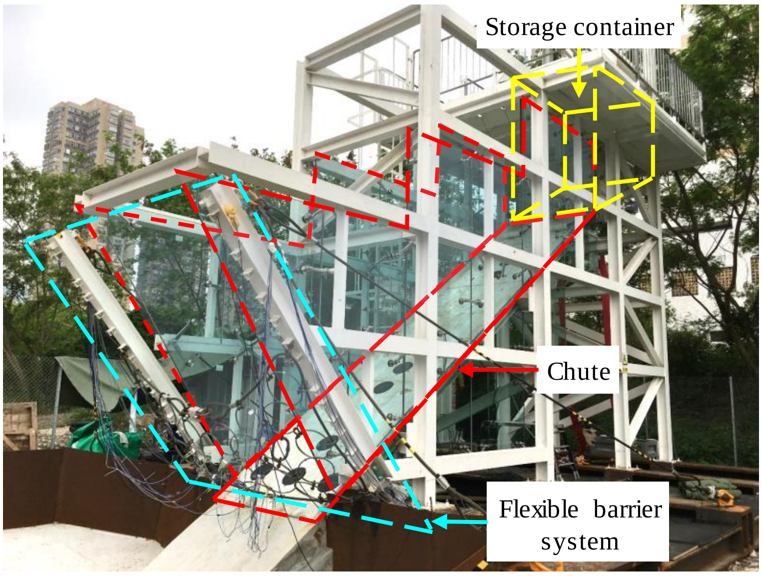

(a)

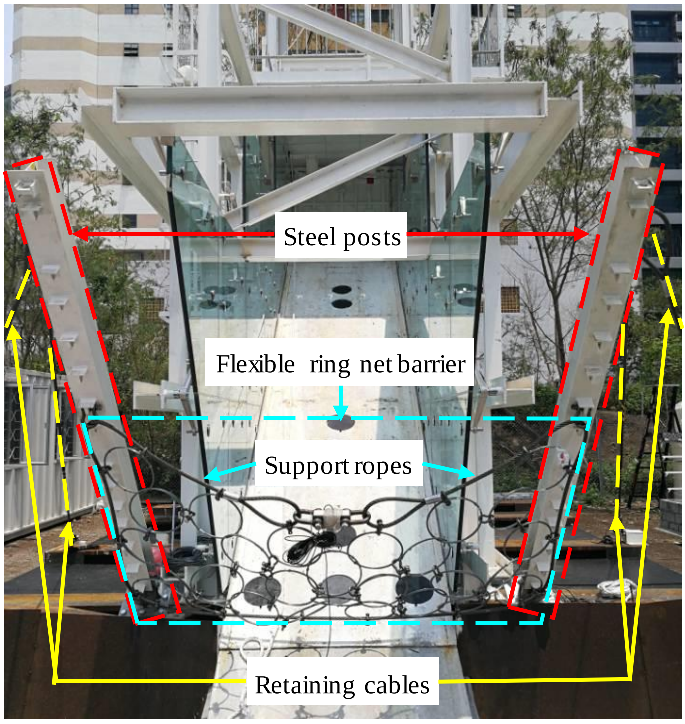

(b)

Fig. 4. Panorama of (a) the large-scale physical model for testing a flexible barrier under impact of a single boulder or debris flow and (b) the flexible barrier system.

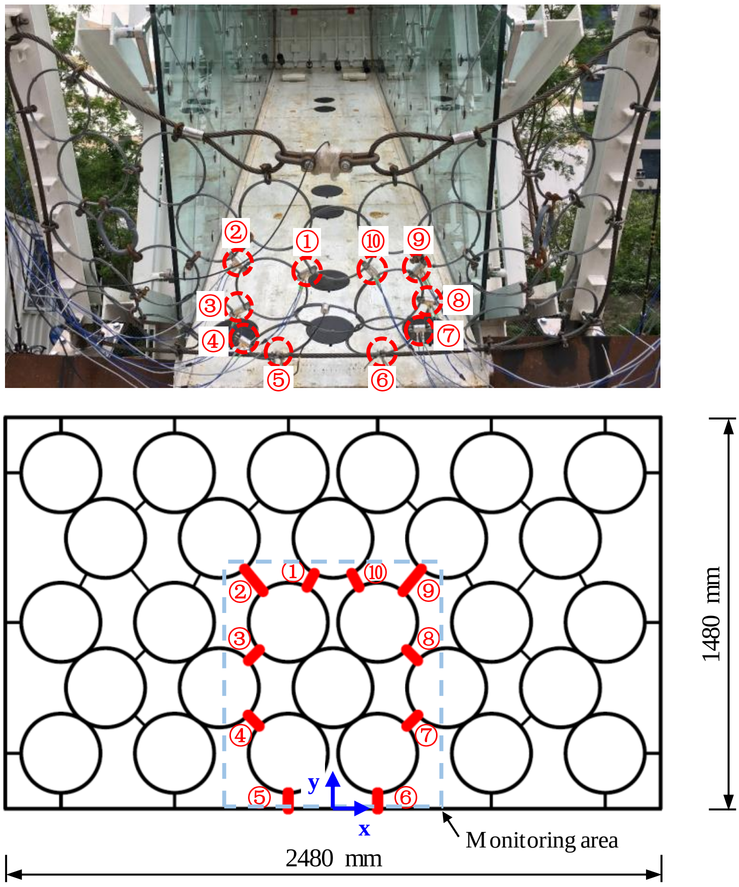

(a)

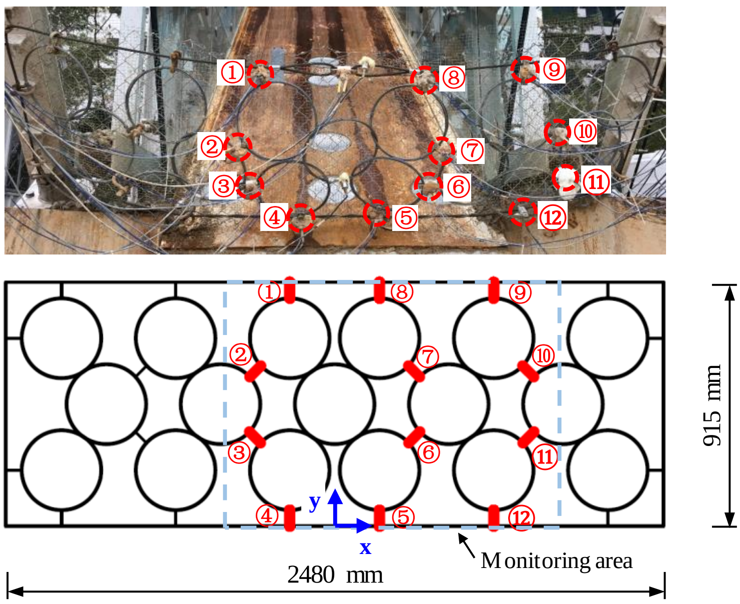

(b)

Fig. 5. Arrangement of FBG mini tension link transducers in a flexible barrier: (a) the single boulder impact test and (b) the debris flow impact test

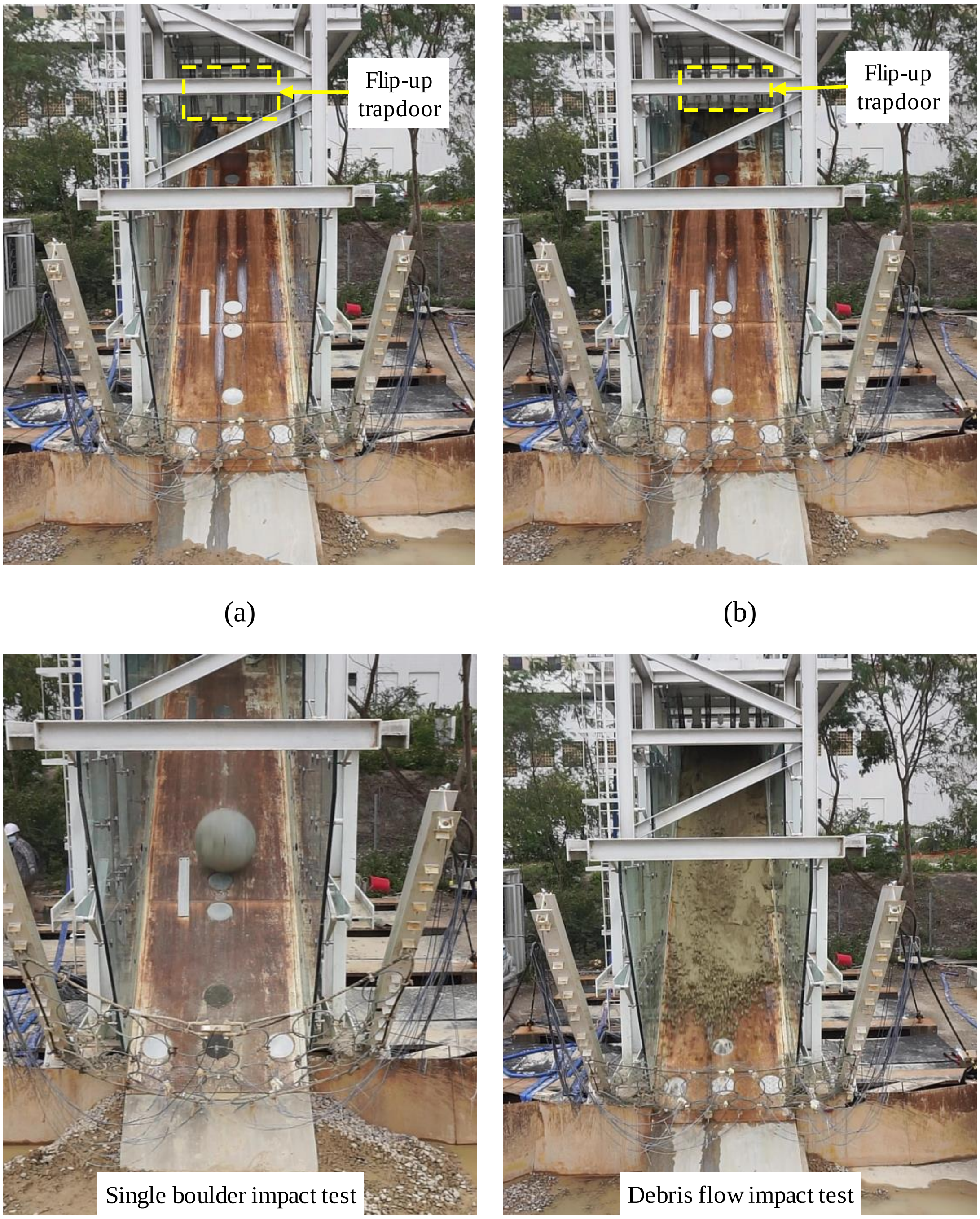

(c)

Fig. 6. Experimental process: (a) before test, (b) door flipping up, and (c) material releasing

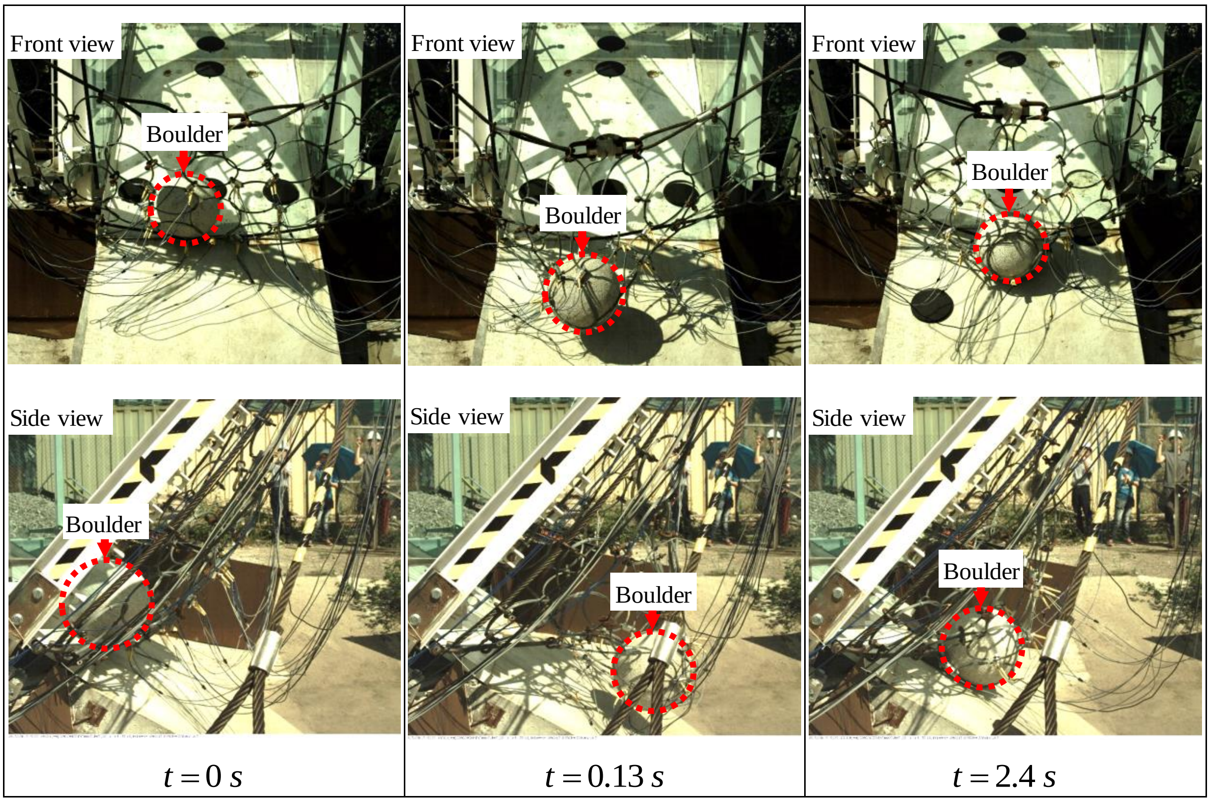

(a)

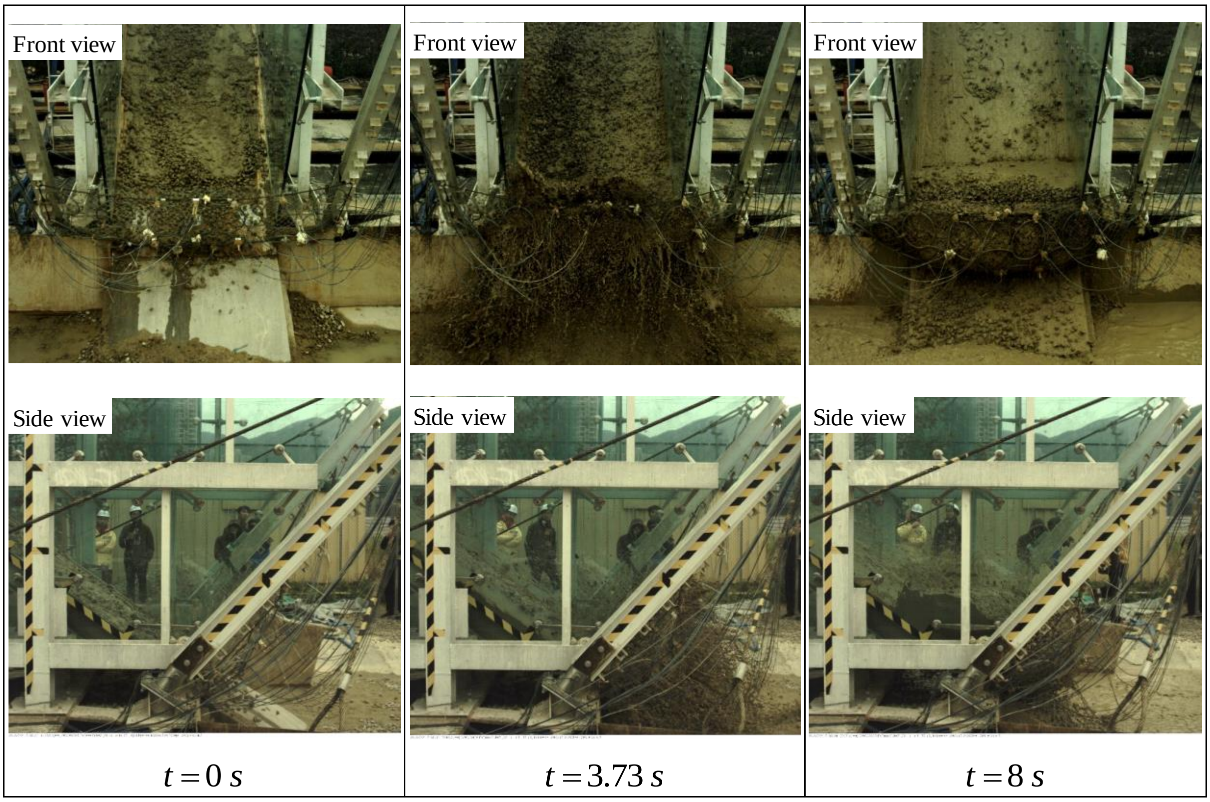

(b)

Fig. 7. Typical video recordings for: (a) the single boulder impact test and (b) the debris flow impact test

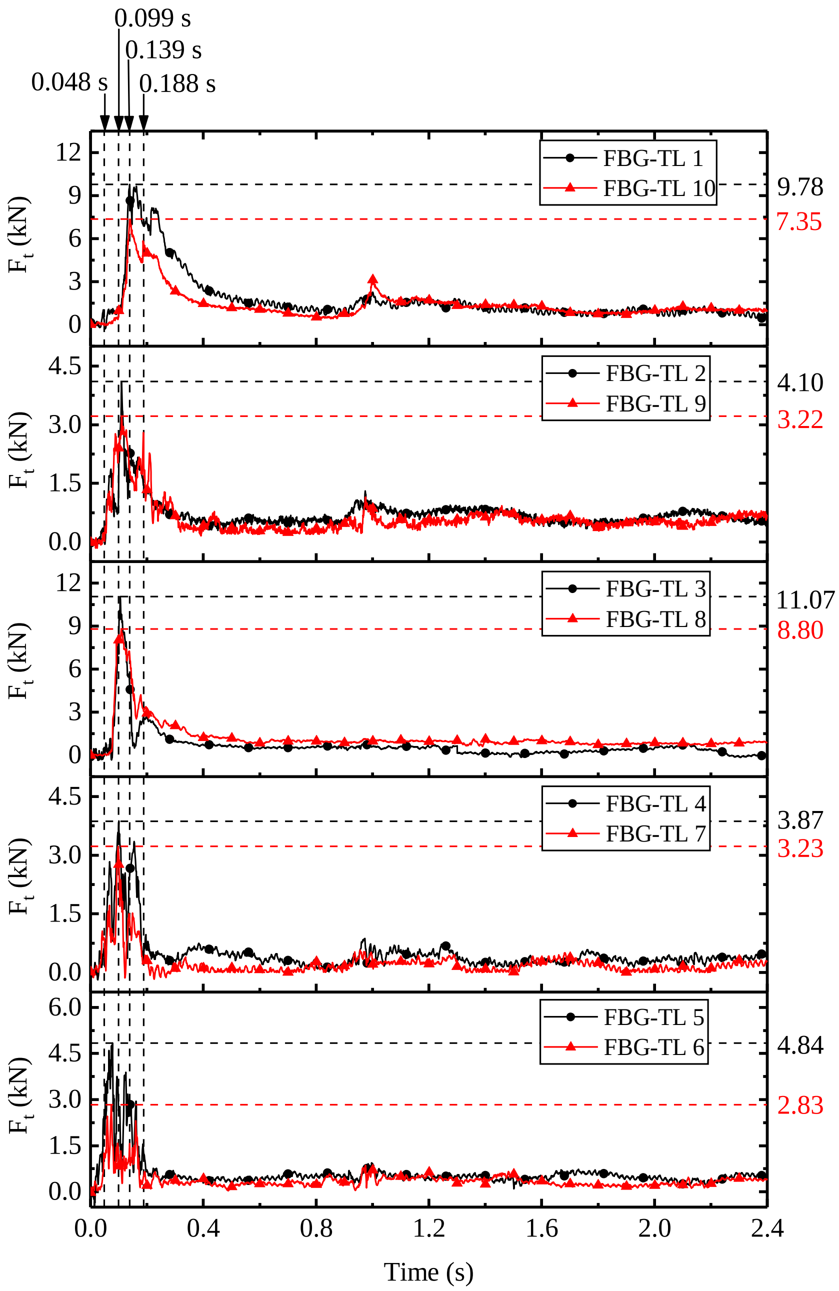

Fig. 8. Time histories of the measured forces (F_t) between rings of the flexible barrier for the single boulder impact test

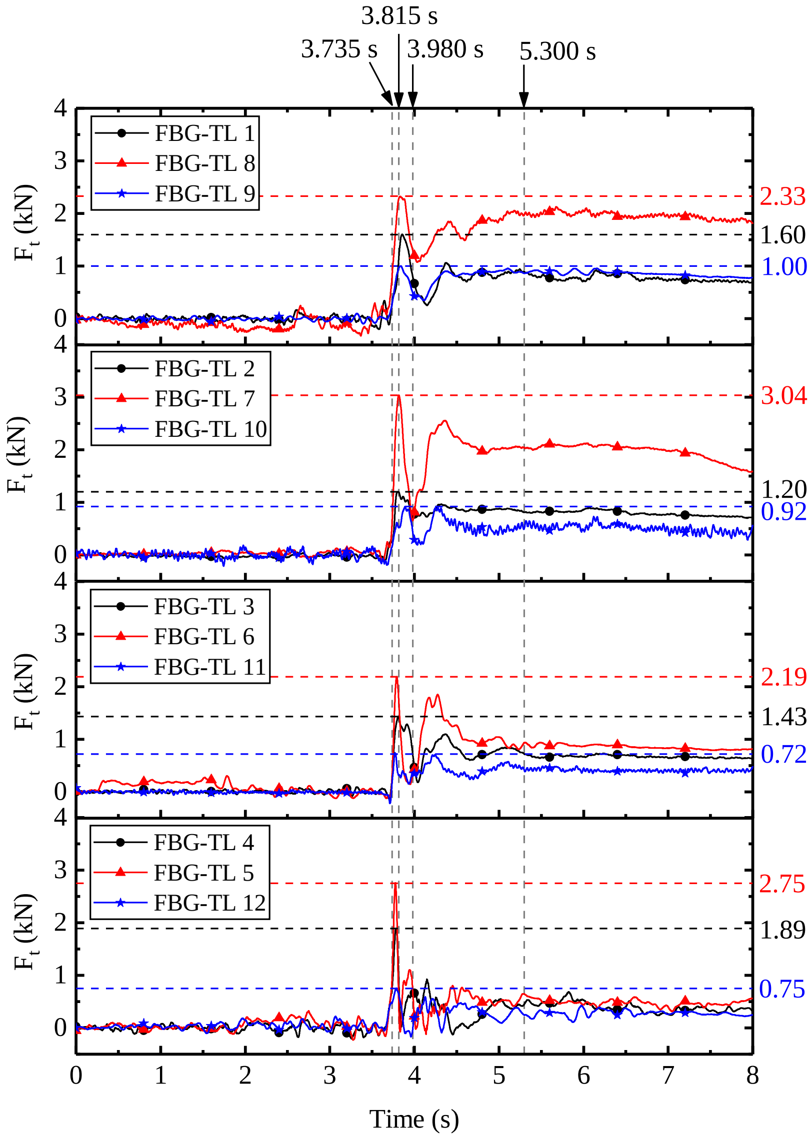

Fig. 9. Time histories of the measured forces (F_t) between rings of the flexible barrier for the debris flow impact test

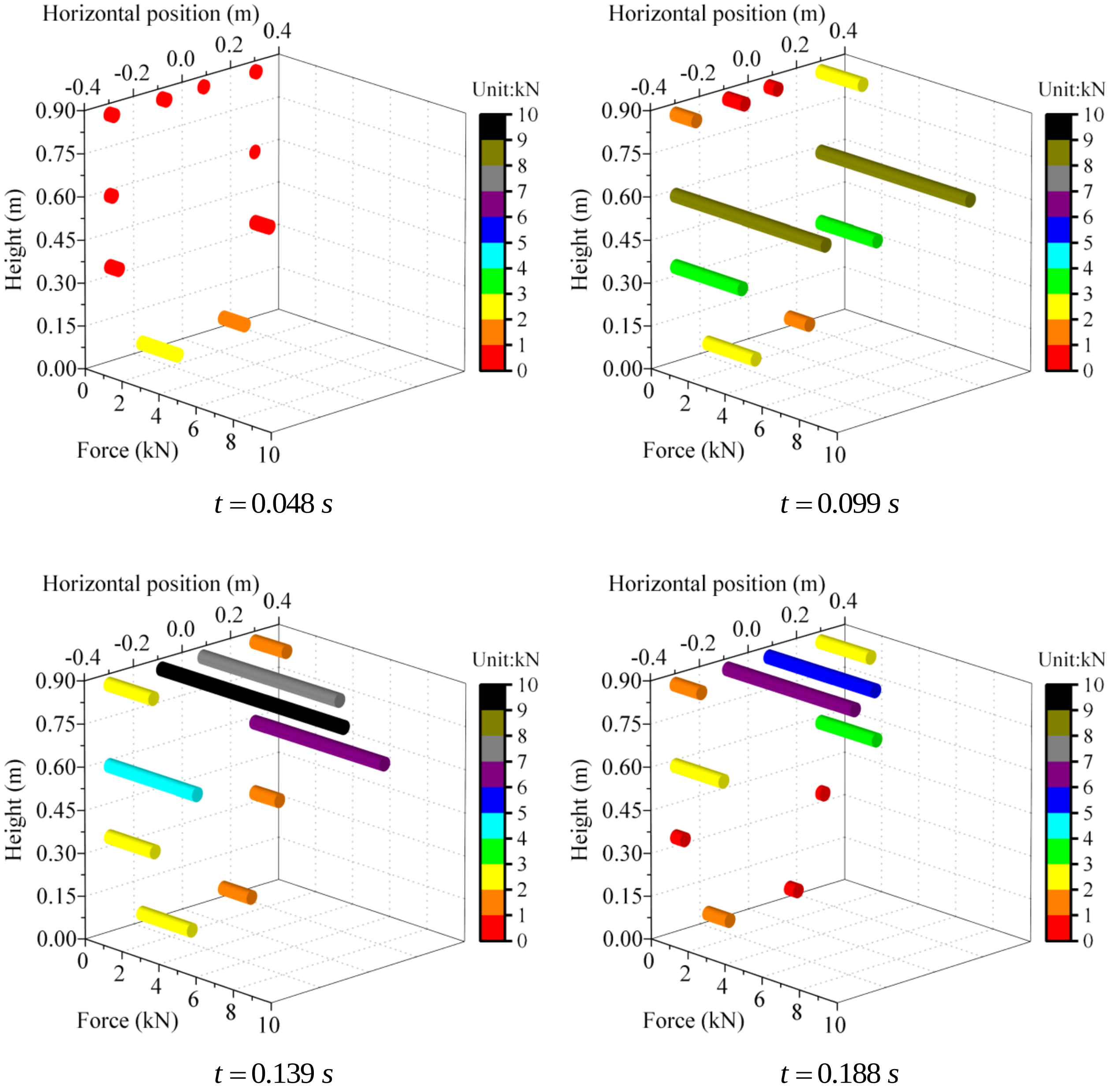

Fig. 10. Distribution of the forces between rings of the flexible barrier for the single boulder impact test

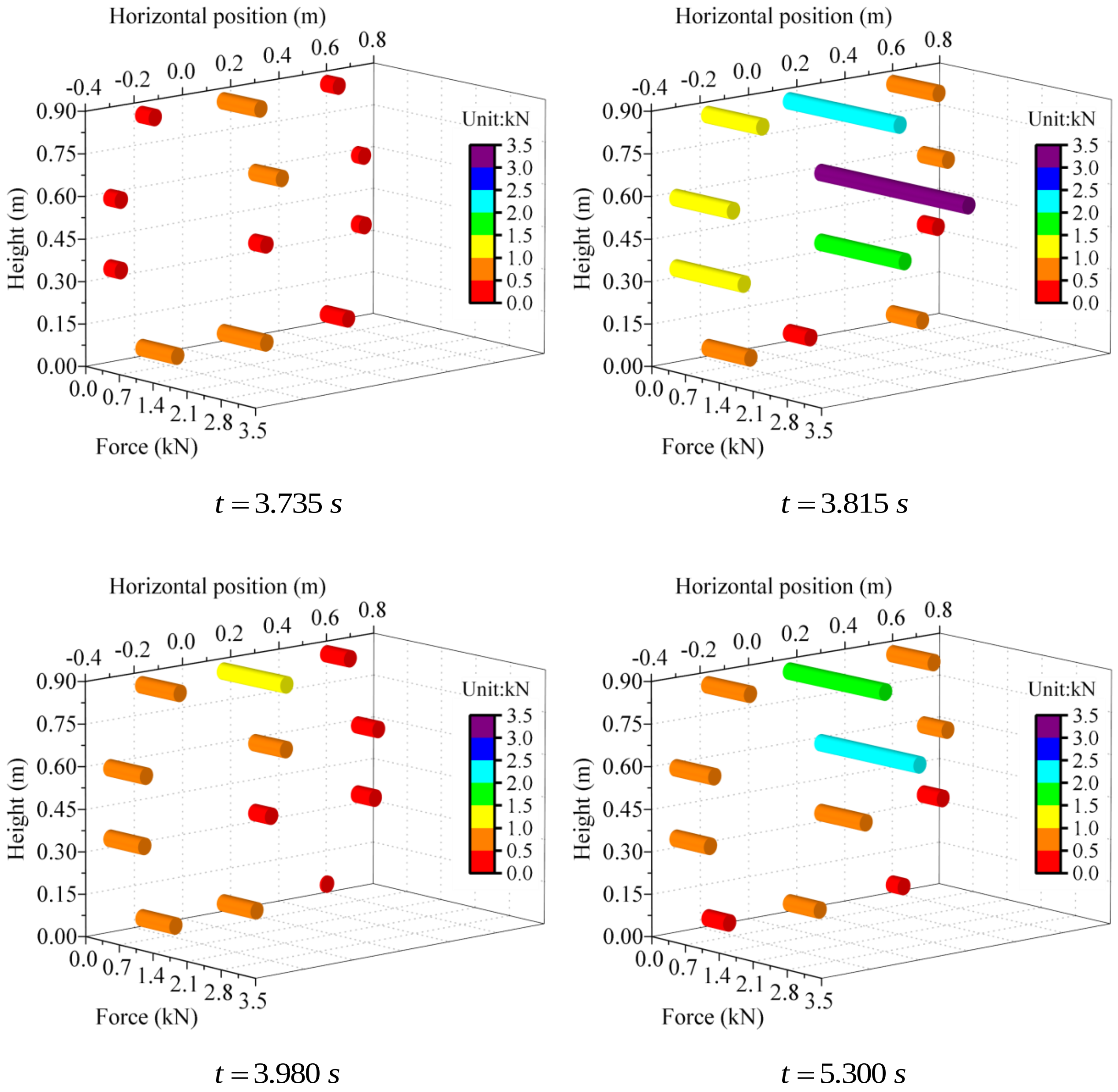

Fig. 11. Distribution of the forces between rings of the flexible barrier for the debris flow impact test

Table(s)

Table 1 Comparison of the coefficients obtained from calibration results and theoretical calculations for the FBG mini tension link transducers (FBG-TL 1/2/3)

	Wavelength λ_{B0} (nm)	**Coefficient** C_F (kN/nm)		**Relative error** E_R (%)
		Calibration results	Theoretical calculations	
FBG-TL 1	1525.658	34.01	32.94	3.25
FBG-TL 2	1540.653	33.67	32.62	3.22
FBG-TL 3	1555.651	33.33	32.31	3.16